Journal of GeoEngineering, Vol. 9, No. 1, pp. 11-19, April 2014
http://dx.doi.org/10.6310/jog.2014.9(1).2

SLOPE DISPLACEMENT ANALYSES USING FORCE EQUILIBRIUM-BASED FINITE DISPLACEMENT METHOD AND CIRCULAR FAILURE SURFACE

Ching-Chuan Huang [1], Horng-Yue Hsieh [2], and Yun-Lung Hsieh [3]

ABSTRACT

Conventional methods of slope stability provide a constant value for the safety factor of the slope, without information of slope displacements and possible variations of safety margins along the potential failure surface. To overcome this shortcoming, a force-equilibrium-based finite displacement method (FFDM) is proposed. Two well known slice methods for circular failure surfaces, namely, the simplified Bishop's and Fellenius' methods are considered in the proposed procedure. The FFDM takes into account all limit equilibrium requirements originally adopted in the slice method with additional displacement compatibility functions and hyperbolic shear stress-displacement relationships. The FFDM provides incremental slope displacements induced by internal or external stress (or safety status) variations. The FFDM also provides local stress-based and displacement-based safety factors as parts of analytical outputs. A monitored highway slope during a rainstorm is used in a preliminary verification of FFDM. Results of the comparative study shows that the slope displacements computed using Fellenius' approach tend to be over-conservative, regardless of different considerations on the influence of groundwater pressures, due partially to its less realistic assumption on the inter-slice forces. The simplified Bishop's method provides acceptable analytical slope displacement results comparable with that measured for the studied slope caused by an elevated groundwater, and is recommended for further applications.

Key words: Slope stability, slope displacement, rainfall-induced slope displacement, limit equilibrium, slice method, displacement compatibility, hyperbolic soil model.

1. INTRODUCTION

The problem of slope instability is an everlasting challenge to the societies of geosciences and civil engineering. Various methods of slope stability using limit equilibrium, finite element, and other methods are frequently reported (Duncan and Wright 2005). Under the framework of limit equilibrium, Fellenius pioneered the slice method of slope stability in the 1920's (Fellenius 1936). Fellenius' original method and the updates that followed constituted a major contribution to the practice and development of geotechnical engineering. (Bishop 1955; Mogenstern and Price 1965; Janbu 1973; Sarma 1973; Spencer 1973). It is well-known that the groundwater table rise and rainfall infiltration have been recognized as major factors that cause slope instability (Leshchinsky and Huang 1992; Huang 2013a, b). Current slice methods of slope stability can provide only limited information regarding the rainfall-induced slope instability, *i.e.*, only the changes of safety factors caused by the rainfall infiltration or groundwater table rise, can be obtained as an outcome of analyses. To this end, the simplified Bishop's and Fellenius' slice methods of slope stability will be used here as examples for the FFDM formulations. It is noted that the principle and equations proposed here are equally effective to other slice methods regardless of their numerical accuracies and shapes of failure surface. An example of applying this approach to a generalized slice method has been reported by Huang (2013a, b).

Figure 1 schematically shows a potential failure mass with ns vertical slices, in which W_i, N_i and S_i represent self-weight, the normal force at the base, and the shear force at the base of slice i, respectively. Forces acting on a typical slice i are shown in Figs. 2(a) and 2(b) for Fellenius' and Bishop's methods, respectively. Based on the simplified Bishop's method, a safety factor (F_s) for the slope can be expressed as:

$$F_s = \frac{\sum \left[C_i + (W_i - U_i \cos\alpha_i) \cdot \tan\varphi \cdot \sec\alpha_i \right] \Big/ \left(1 + \dfrac{\tan\alpha_i \cdot \tan\phi}{F_s} \right)}{\sum (W_i \cdot \sin\alpha_i)} \tag{1}$$

where

C_i : Cohesive shear resistance at the base of slice i ($= c \cdot \ell_i = c \cdot B_i \cdot \sec\alpha_i$)

U_i : Uplifting force acting at the base of slice i ($= u_i \cdot \ell_i = u_i \cdot B_i \cdot \sec\alpha_i$)

Manuscript received November 27, 2013; revised February 24, 2014; accepted February 27, 2014.

[1] Professor (corresponding author), Department of Civil Engineering, National Cheng Kung University No. 1, University road, Tainan, Taiwan, 70101 (e-mail: samhcc@mail.ncku.edu.tw).

[2] Graduate student, Department of Civil Engineering, National Cheng Kung University No. 1, University road, Tainan, Taiwan, 70101.

[3] Graduate student, Department of Civil Engineering, National Cheng Kung University No. 1, University road, Tainan, Taiwan, 70101.

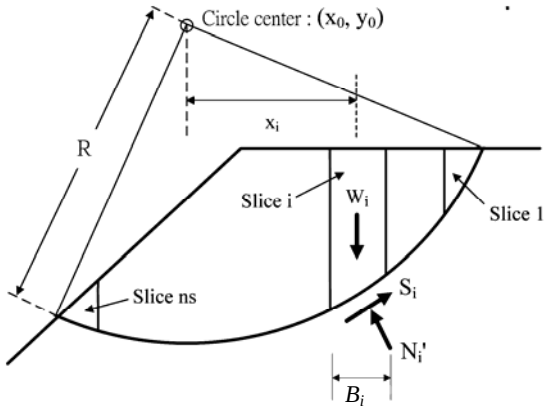

Fig. 1 A potential failure mass confined by a circular failure surface

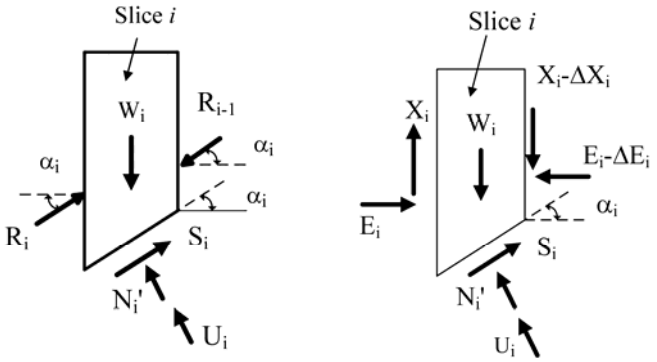

(a) Fellenius' method (b) Bishop's method

Fig. 2 Forces acting on a typical slice *i*

i : Slice number (i = 1, 2, …, ns)
W_i : Self-weight of slice i
α_i : Inclination angle of slice base i
c : Cohsion intercept of soil
ϕ : Internal friction angle of soil
u_i : Porewater pressure acting at slice base i
ℓ_i, B_i : The length of base and the width, respectively, for slice i.

Note that in Eq. (1), a differential term of vertical inter-slice force, ΔX_i (= $X_i - X_{i-1}$; X_i, X_{i-1}: Vertical inter-slice forces acting on the left and right sides, respectively, of slice i) is ignored (or $\Delta X_i = 0$ is assumed).

In the Fellenius' method, the force equilibrium in the direction normal to the slice base ($\Sigma F_N = 0$) does not take into account the influence of inter-slice forces. This method is based on the implicit assumption that the resultant inter-slice force acts parallel to the slice base. F_s is expressed as:

$$F_s = \frac{\sum\left[C_i + (W_i \cdot \cos\alpha_i - U_i)\cdot \tan\phi\right]}{\sum(W_i \cdot \sin\alpha_i)} \tag{2}$$

It is well-known that values of F_s obtained from Eq. (2) are conservative compared with those obtained from rigorous slice methods, because of the less realistic assumptions regarding the inter-slice forces (Whitman and Bailey 1967; Leshchinsky and Huang 1992). It is also well known that the conservatism of the Fellenius' method can be improved by using the concept of buoyant weight of soils (Whitman and Bailey 1967). In this case, the F_s can be expressed as:

$$F_s = \frac{\sum(C_i + W_i' \cdot \cos\alpha_i \cdot \tan\phi)}{\sum(W_i \cdot \sin\alpha_i)} \tag{3}$$

where

W_i' : Buoyant weight of slice i

2. DERIVATION OF FORCE-EQUILIBRIUM-BASED FINITE DISPLACEMENT METHOD

In the Bishop's method, the effective normal force N_i' can be expressed based on the force equilibrium in the direction of gravity (*i.e.*, $\Sigma F_V = 0$) and the assumption of $\Delta X_i = X_{i-1} - X_i = 0$, as schematically shown in Fig. 2(b) (Bishop 1955):

$$N_i' = (W_i - S_i \cdot \sin\alpha_i - U_i \cdot \cos\alpha_i)\cdot \sec\alpha_i \tag{4}$$

In the Fellenius' method, effective normal force N_i' is derived based on the principle of the force equilibrium normal to the slice base (*i.e.*, $\Sigma F_N = 0$) and the assumption that the resultant inter-slice forces are parallel to the slice base (as schematically shown in Fig. 2(a)):

$$N_i' = W_i \cdot \cos\alpha_i - U_i \tag{5}$$

It is empirically known that taking into account the effect of up-lifting force U_i as shown in Eq. (5) may generate overly conservative results. To this end, Baily and Whitmann (1967) suggested that N_i' can be derived using the concept of buoyant weight:

$$N_i' = W_i' \cdot \cos\alpha_i \tag{6}$$

In the proposed FFDM, a local stress-based safety factor FS_i is defined according to the Mohr-Coulomb's failure criterion. Note that the local FS_i is different from the averaged (or constant) value of F_s used in conventional limit equilibrium methods such as those shown in Eqs. (1) ~ (3).

$$FS_i = \frac{\tau_{fi}}{\tau_i} = \frac{S_{fi}}{S_i} = \frac{C_i + N_i' \cdot \tan\phi}{S_i} \tag{7}$$

$$S_{fi} = \tau_{fi} \cdot \ell_i = C_i + N_i' \cdot \tan\phi \tag{8}$$

$$S_i = \tau_i \cdot \ell_i \tag{9}$$

where

τ_{fi}, τ_i : Ultimate shear strength, and shear stress, respectively, for slice i.
S_{fi}, S_i : Ultimate shear resistance and shear force, respectively, for slice i
FS_i : Local force-based safety factor

As is shown in Fig. 3, the shear stress (τ_i) vs. shear dis-

placement (Δ_i) relationship is represented by a hyperbolic curve which constitutes the mechanical foundation of the proposed method:

$$\tau_i = \frac{\Delta_i}{a' + b' \cdot \Delta_i} \tag{10}$$

where

$$a' = \frac{1}{k_{initial}} \tag{11}$$

$$b' = \frac{R_f}{\tau_{fi}} \tag{12}$$

$$k_{initial} = K \cdot G \cdot \left(\frac{\sigma'_{n_i}}{P_a} \right)^n \tag{13}$$

$$\sigma'_{n_i} = \frac{N'_i}{B_i \cdot \sec \alpha_i} \tag{14}$$

where

$k_{initial}$: Initial shear stiffness
K, n : Material constants
R_f : Failure ratio
σ'_{n_i} : Normal stress acting at the base of slice i
P_a : Atmospheric pressure (= 101.3 kPa)
G : Reference stiffness (= 101.3 kPa/m)

Normalizing Eq. (10) using τ_{fi}:

$$\frac{\tau_i}{\tau_{fi}} = \frac{\Delta_i}{a + b \cdot \Delta_i} \tag{15}$$

$$a = a' \cdot \tau_{fi} = \frac{\tau_{fi}}{k_{initial}} \tag{16}$$

$$b = b' \cdot \tau_{fi} = R_f \tag{17}$$

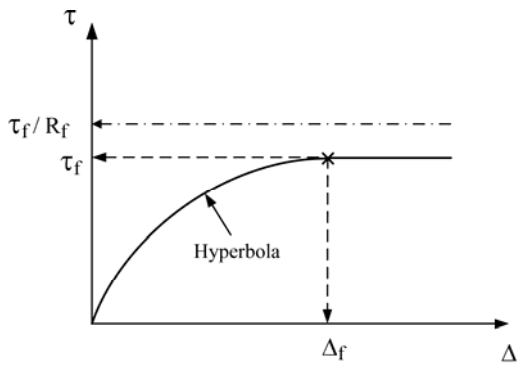

Fig. 3 Hyperbolic model of shear displacement *vs.* shear stress for soils

Based on the definitions of local safety factors in Eq. (7), Eq. (15) can be re-written as:

$$FS_i = \frac{a + b \cdot \Delta_i}{\Delta_i} \tag{18}$$

A displacement diagram (Atkinson 1981) that satisfies displacement compatibility as schematically shown in Figs. 4(a) and 4(b) can be introduced:

$$\Delta_2 = \Delta_1 \cdot \frac{\cos(\alpha_1 - 2\psi)}{\cos(2\psi - \alpha_2)} \tag{19}$$

where

ψ: Dilatancy angle of soils

The displacement of slice i can be related to the vertical displacement at the top of slice 1 (Δ_o) using the following equation:

$$\Delta_i = \Delta_1 \cdot \frac{\cos(\alpha_1 - 2\psi)}{\cos(2\psi - \alpha_i)} = \frac{\Delta_o}{\sin(\alpha_1 - \psi)} \cdot \frac{\cos(\alpha_1 - 2\psi)}{\cos(2\psi - \alpha_i)} \tag{20}$$

Equation (20) can be expressed as:

$$\Delta_i = \Delta_o \cdot f(\alpha_i) \tag{21}$$

where

$$f(\alpha_i) = \frac{1}{\sin(\alpha_1 - \psi)} \cdot \frac{\cos(\alpha_1 - 2\psi)}{\cos(2\psi - \alpha_i)} \tag{22}$$

Substitute Eq. (21) into Eq. (18),

$$FS_i = \frac{a + b \cdot \Delta_o \cdot f(\alpha_i)}{\Delta_o \cdot f(\alpha_i)} \tag{23}$$

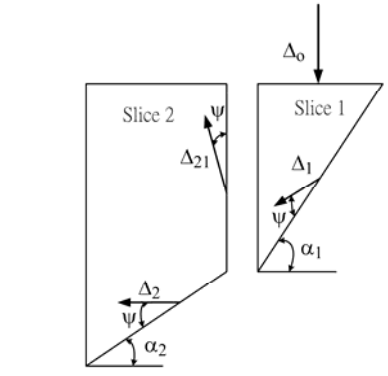

(a) Vectors of shear displacement

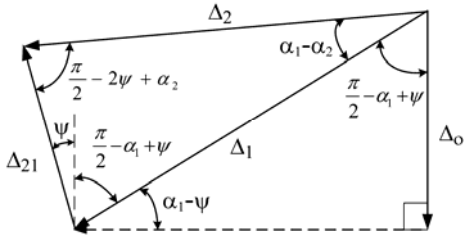

(b) Displacement diagram

Fig. 4 Displacement compatibility of adjacent slices

Based on the principle of moment equilibrium at the center of circle, *i.e.*, $\Sigma M_O = 0$:

$$\sum \frac{C_i + N' \cdot \tan\varphi}{FS_i} = \sum (W_i \cdot \sin\alpha_i) \tag{24}$$

Substitute Eq. (23) into Eq. (24), a close-form solution of Δ_O can be expressed as:

$$\Delta_o = \frac{\sum (W_i \cdot \sin\alpha_i)}{\sum [C_i + N' \cdot \tan\phi] \cdot \left[\dfrac{f(\alpha_i)}{a + b \cdot \Delta_o \cdot f(\alpha_i)} \right]} \tag{25}$$

In Eq. (25), various values of N' expressed by Eqs. (4) and (5) (or Eq. 6) can be used to compute Δ_0 for simplified Bishop's and Fellenius' methods, respectively. It can be seen that Eq. (25) is basically a reversed expression of Eqs. (1) and (2), with known displacement-related parameters '*a*', '*b*', '$f(\alpha_i)$', and the unknown 'Δ_o'. It is also noted that the unknown 'Δ_o' appears at both sides of the equation, indicating that an iterative procedure is required in calculating values of 'Δ_o'. This situation is similar to that used for deriving the safety factor using the simplified Bishop's method (Bishop 1955) which also requires iterative calculations for the safety factor of the slope. A criterion of $\varepsilon = 1\%$ is used here to detect the convergence of Δ_0:

$$\frac{(\Delta_o)_{new} - (\Delta_o)_{old}}{(\Delta_o)_{new}} \le \varepsilon \tag{26}$$

3. LOCAL DISPLACEMENT-BASED SAFETY FACTORS

The displacement at failure (Δ_f) can be obtained by using $FS_i = 1.0$ in Eq. (18):

$$FS_i = \frac{a + b \cdot \Delta_f}{\Delta_f} = 1.0 \tag{27}$$

Re-arrange the above equation to obtain Δ_f:

$$\Delta_f = \frac{a}{1 - b} \tag{28}$$

A displacement-based safety factor, FD_i can be defined as:

$$FD_i = \frac{\Delta_f}{\Delta_i} \tag{29}$$

$$FD_i = \frac{a}{\Delta_o \cdot f(\alpha_i) \cdot (1 - b)} \tag{30}$$

The hyperbolic stress-displacement relationship used in the present study can be easily modified for special cases, *e.g.*, linearly elastic pre-peak with a post-peak (residual) strength or hyperbolic pre-peak with post-peak strength. These issues are beyond the scope of the present study.

4. INCREMENTS OF SLOPE DISPLACEMENT AND COMPUTER FLOW CHART

In calculating slope displacements induced by external and internal condition changes (*e.g.*, loading, water table, and porewater pressure variations), two values of Δ_i (or Δ_0), namely, pre-rainfall slope displacement (Δ_i^a) and post-rainfall slope displacement (Δ_i^b), should be calculated, and the increment of displacement for slice *i*, induced by the rainfall event is schematically shown in Fig. 5, and is defined as:

$$\Delta_i = \Delta_i^b - \Delta_i^a \tag{31}$$

Figure 5 shows one of the possible stress paths for a soil element on the potential failure surface subjected to a rainfall-induced groundwater table rise. In this case, the shear stress on the element is largely remain unchanged because the porewater-pressure-independent character of shear stresses (or deviatoric stresses), and the increase of soil self-weight of soil from a moist condition to a saturated one is usually small. On the other hand, the effective normal pressure (σ_n) on the potential failure surface is reduced due to the increase of porewater pressure. Therefore, an incremental displacement responding to the decrease of σ_n occurs, as shown in Fig. 5. A summary of unknowns and equations in the proposed FFDM is shown in Table 1 which also indicates that the proposed method is in a static determinate condition. A computer program was coded in Visual Basic Express 2010 (Microsoft 2010) for computing slope displacements induced by external and/or internal factor changes. The flow chart is shown in Fig. 6.

5. CASE STUDY

The studied slope was located in the southwest foothills of Taiwan. The slope was a part of highway No. 18, which winds through an area prone to landslides. Landslides cause property losses and traffic problems in this area during the rainy seasons. Therefore, this area has been closely monitored and studied (Chang *et al*. 2005). Figure 7 shows the studied slope with locations of inclinometer measurements, groundwater tables and sliding surface (Energy and Resources Research Laboratory of Industrial Technology Research Institute, ERRL 1999). The observed slip surface is fitted by an arc with a radius of 1543m and a rotation center at (*X*, *Y*) = (49.7m, 1569.5m), which are also shown in the figure. Underground water table observations were conducted in a borehole adjacent to the slope during a rainstorm. According to inclinometer measurements, the slope displacement during typhoon Herb in 1995 was 30mm in the downward direction (ERRL 1999). Site exploration and inclinometer measurements revealed that the sliding slope mass consists of colluviums and rock fragments. The slip surface at inclinometer 04-4 is about 90 m-deep from the ground surface and is located at highly weathered rock strata. Therefore, undisturbed sampling and testing at this depth is difficult. Possible values of ϕ for the matrix materials were estimated in the range of 25° ~ 30° and a cohesion intercept c = 40kPa, according to the back-analysis result reported by ERRL (1999). Figure 8 shows changes in conventional safety factors (F_s) for the studied slope caused by the elevated

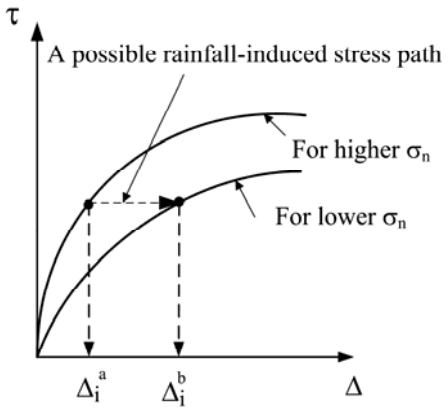

Fig. 5 Shear stress and displacement paths induced by a reduction of normal stress

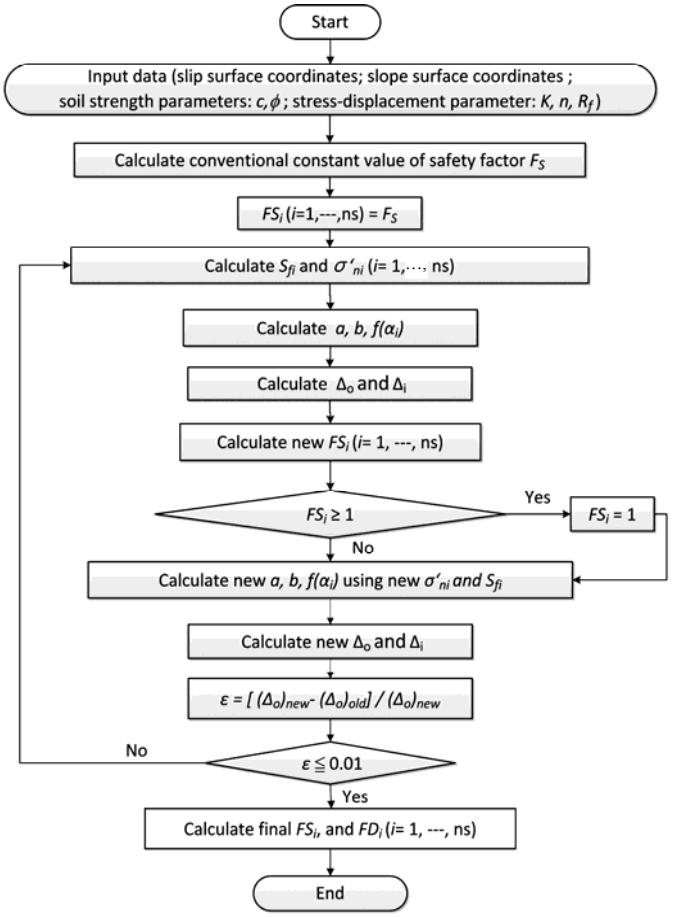

Fig. 6 FFDM computer flow chart (program DISP-SLICE)

groundwater table based on Eqs. (1), (2), and (3). For both Bishop's and Fellenius' methods, reductions in F_s of about 0.05 ~ 0.06 are obtained for an internal friction angle (ϕ) between 25° and 30°, and a cohesion intercept c = 40kPa for above-water-table zone in the pre-rainfall case. Note that conventional limit-equilibrium- based slope stability analyses cannot provide information beyond this point, and a reduction in F_s of 0.05 ~ 0.06 provides limited information about the influence of the groundwater table (or the effect of rainfall) on the performance of the slope.

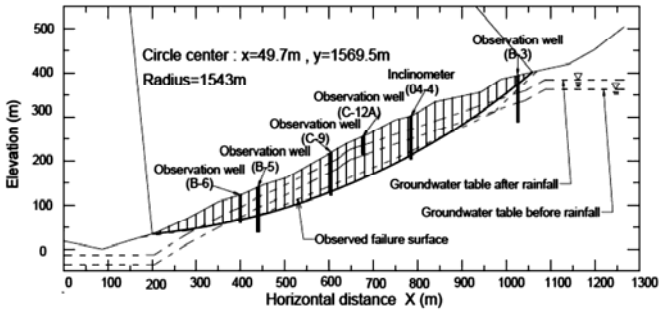

Fig. 7 Cross section of the studied slope

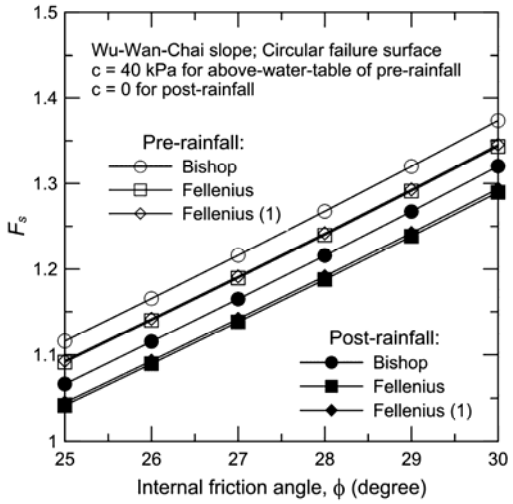

Fig. 8 Conventional safety factors for pre- and post-rainfall conditions

Table 1 Unknowns and equations in the proposed FFDM

Unknown	Number of unknowns	Equation	Number of equations
N_i'	*ns*	$\Sigma F_N = 0$; Eq. (5) $\Sigma F_V = 0$; Eq. (4)	*ns*
S_i	*ns*	$\Sigma M_o = 0$; Eq. (24)	1
FS_i	*ns*	Mohr-Coulomb's failure criterion and definition of FS_i $S_i = \dfrac{C_i + N_i' \tan\varphi}{FS_i}$; Eq. (7)	*ns*
FD_i	*ns*	$FD_i \left(= \dfrac{\Delta_f}{\Delta_i} \right)$; Eq. (30)	*ns*
Δ_i ($i = 2 \sim ns$)	*ns*-1	Stress-displacement relationships (τ_i vs. Δ_i); Eq. (10)	*ns*
Δ_o	1	Displacement compatibility $\Delta_i = \Delta_o \cdot f(\alpha_i)$; Eq. (21) ($i$ = 2---*ns*)	*ns*-1
	5 *ns*		5 *ns*

Although undisturbed sampling and large-scale direct shear tests were not performed for the studied slope, large-scale direct shear tests performed for various soils (Huang 2013(a), (b)) generally suggest the applicability of the hyperbolic shear stress-displacement relationships with model parameters, K in the ranges of 50 and 300; n in the range of 0.1 and 0.3; R_f in the range of 0.7 and 0.9. For a comparative purpose, c = 40kPa, ϕ = 25°, K = 80, n = 0.1, and R_f = 0.8 are used in the following analyses according to the results of parametric study performed by Huang 2013(a); 2013(b). Table 2 shows a comparison of calculated slope displacement at X = 784m where inclinometer 04-4 was installed. Calculating the slope displacements shown in Table 2 involves the following three steps: (1) calculating the vertical displacement at the crest of the potential failure surface, Δ_0 (using Eq. 25) for the pre-rainfall and the post-rainfall conditions; (2) calculating displacements at the targeted location of failure surface (X = 784 m in this study) for pre-rainfall and post-rainfall conditions (namely, Δ_i^a and Δ_i^b) using displacement compatibility function (Eq. 21); (3) calculating incremental slope displacement at the targeted location, induced by the rising of groundwater table, using Eq. (31). It can be seen that simplified Bishop's limit-equilibrium approach (Eq. 1) renders slope displacement value (0.029m) comparable with the measured value of 0.032m. However, this is not the case for the Fellenius limit-equilibrium approach (Eqs. 2 and 3) which generates smaller displacements than the others, despite their different considerations for the effect of porewater pressure.

Figure 9(a) compares local stress- and displacement-based safety factors (FS_i and FD_i) for the case c = 40kPa, ϕ = 25°, K = 80, n = 0.1, and R_f = 0.8. Based on the conventional constant-safety factor concept, values of F_s using simplified Bishop's method, using c = 40kPa; ϕ = 25° for pre-rainfall, and c = 0; ϕ = 25° for post-rainfall conditions, are 1.12 and 1.06, respectively, as shown in Fig. 8. The use of c = 0kPa in the analyses for the post-rainfall condition is based on a well-known phenomenon of rainfall infiltration which penetrates from the slope surface down toward the existing groundwater table via the so-called "wetting front propagation", leading to a near-saturated (or c = 0) condition of the slope. Distributions of FS_i and FD_i for the pre-rainfall case reveal that a major part of the potential failure surface are associated with $FS_i > 1$ (or $FD_i > 1$). Only small portions of the potential sliding mass (close to the toe and the crest of potential failure mass) were associated with $FS_i < 1.0$ (or $FD_i < 1.0$) conditions. In the case of post-rainfall, the slope experienced substantial drops in FS_i and FD_i, for a major portion of the failure surface. It can be seen that part of the slices experience FS_i = 1.0, indicating that ultimate failure conditions have been reached at these locations. This observation is consistent with observations that tension cracks developed around the crest of sliding mass (Ching and Fredlund 1983; ERRL 1999), and is also consistent with the progressive failure mechanism proposed by Bjerrum (1967), in the sense that a stress re-distribution along the potential failure surface propagates from the slope toe due to the removal of the slope toe. In the present study it is shown that a critical condition occurs at the slope toe because of the combined effects of a high groundwater table and low overburden pressure.

Table 2 Comparisons of calculated horizontal slope displacement at X = 784m for the studied slope (Wu-Wan-Chai slope) based on various slice methods (c = 40kPa for pre-rainfall; c = 0 for post-rainfall, and ϕ = 25°, K = 80, n = 0.1, R_f = 0.8, ψ = 0° , 12.5° for pre- and post-rainfall conditions)

	ψ = 0°	ψ = 12.5°
Simplified Bishop; Eq. (1)	0.029m	0.029m
Fellenius; Eq. (2)	0.013m	0.011m
Fellenius; Eq. (3)	0.011m	0.010m

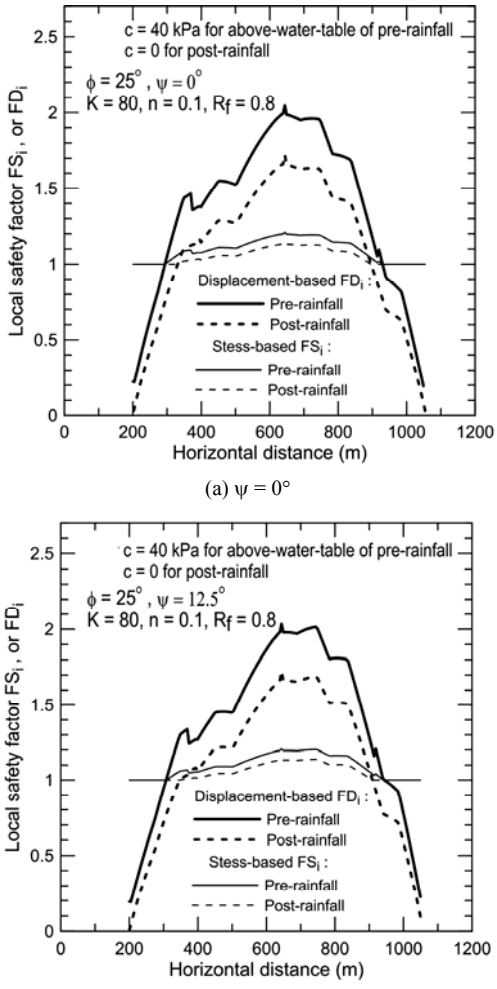

Fig. 9 Local stress-based and displacement-based safety factors using FFDM with Bishop's limit equilibrium approach

It is important to note that the use of displacement-based safety factors, FD_i, seems to be more advantageous than the use of stress-based FS_i, in the sense that the difference in FD_i between the pre-rainfall and post-rainfall cases is larger than that for FS_i. This allows for a more detailed investigation of the safety status of the slope than that based on the FS_i distribution. Figure 9(b)

shows the effect of ψ on the calculated values of FS_i and FD_i by using input conditions identical to those used in Fig. 9(a), except that $\psi = 12.5°$ (= $\phi/2$) is used for Fig. 9(b). Differences between Figs. 9(a) and 9(b) can be hardly seen, indicating that input values of ψ have a negligible influence on the outcomes of FS_i and FD_i. As seen in Figs. 9(a) and 9(b), the stress-based safety factors are with relatively small variations along the entire failure surface. Large variations of the displacement-based safety factors are caused by the non-linear stress- displacement curve used here, *i.e.*, when approaching plastic failure states, a small stress increase can lead to a significant displacement response. This can be deemed as a major advantage of the displacement-based safety factors used in the proposed method.

Figure 10(a) shows the calculated values of shear displacement (Δ_i) and horizontal displacement [$= \Delta_i \cdot \cos(\alpha_i - \psi)$] along the slip surface for the same case shown in Fig. 9(a). Shear displacements at close-to-crest locations are larger than those at close-to-toe locations. It can be seen that horizontal shear displacements along the entire slip surface are identical, suggesting a rigid sliding mass in this case. The case shown in Fig. 10(b) utilizes input parameters similar to those used for Fig. 10(a), except that $\psi = 12.5°$ is used in Fig. 10(b). The influence on the patterns of displacement along the failure surface is significant. By using a non-zero value of $\psi = 12.5°$, the assumption of a rigid body becomes invalid, and the pattern of the shear displacement mimics that of $f(\alpha_i)$, as shown in Fig. 11. The non-uniform displacement behavior shown in Fig. 10(b) reveals another advantage of the proposed method, in the sense that various displacement patterns of the sliding mass can be simulated via the input value of ψ, which dictates the shape of the displacement compatibility function $f(\alpha_i)$.

Figure 12(a) shows typical examples of mobilized shear and effective normal forces along the sliding surface based on identical soil parameters for Figs. 9(a) and 10(a). Distributions of σ'_{n_i} and τ_i generally show significant internal stress distributions, in the sense that normal stresses along the failure surface increase as the depth of the failure surface increases. This trend is consistent with previous studies on the internal stress along the failure surface (Leshchinsky 1990; Leshchinsky and Huang 1992). Increases in σ'_{n_i} and τ_i induced by rainfall (or the rises in the water table) are highlighted in Fig. 12(b). Reductions in σ'_{n_i}, associated with increases of τ_i along a major part of the sliding surface can be seen. In Fig. 12(b), a normal stress reduction of about 20 kPa prevails along the majority of the slip surface. Increases in shear stress are insignificant for a large portion of the slip surface. At close-to- toe and close-to-crest locations where the values of FS_i have reached the critical condition (= 1.0), the slope experienced certain degrees of shear stress reductions, which were caused by the stress re-distribution mechanism.

Figures 13(a) and 13(b) show stresses and stress increments, respectively, for the same case presented in Figs. 12(a) and 12(b). The only difference between Figs. 12 and 13 is the input dilatancy angle (ψ). In this comparison, $\psi = 0°$ and $\psi = \phi/2 = 12.5°$ are used for Figs. 12 and 13, respectively. Comparing Figs. 12 and 13, hardly any difference can be seen, suggesting that input value of ψ (within the investigated range) has a non-detectable influence on the normal and shear stresses distributions (and stress increments) along the failure surface for the investigated slope.

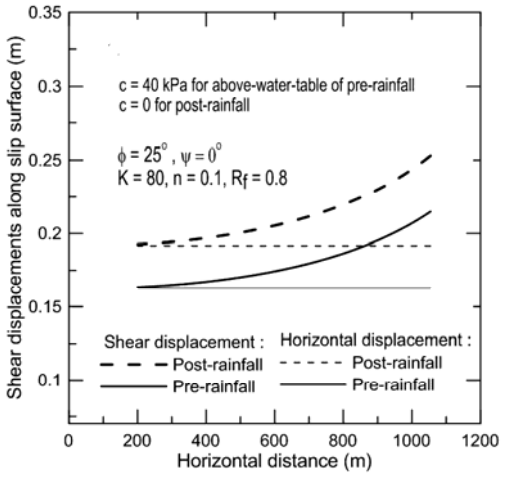

(a) $\psi = 0°$

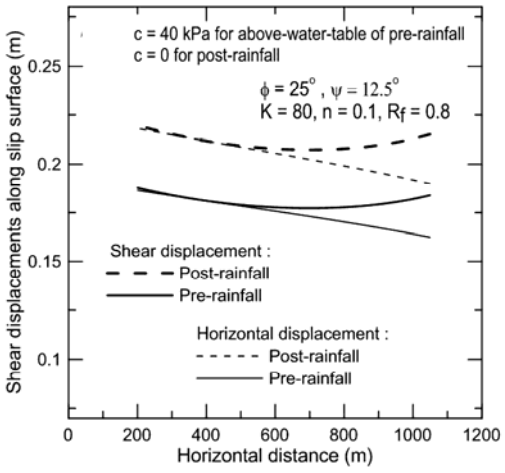

(b) $\psi = 12.5°$

Fig. 10 Shear displacements calculated using FFDM with Bishop's limit equilibrium approach

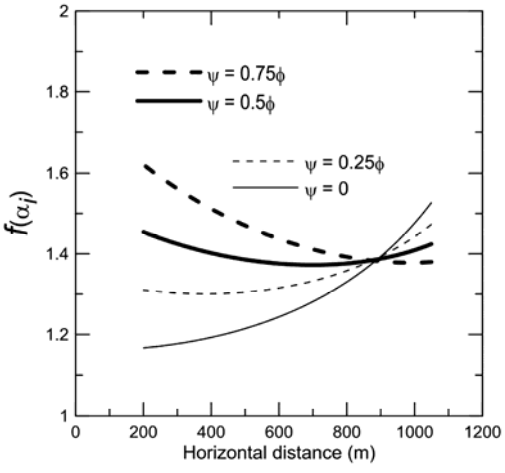

Fig. 11 Variations of $f(\alpha_i)$ induced by various values of ψ for the studied slope

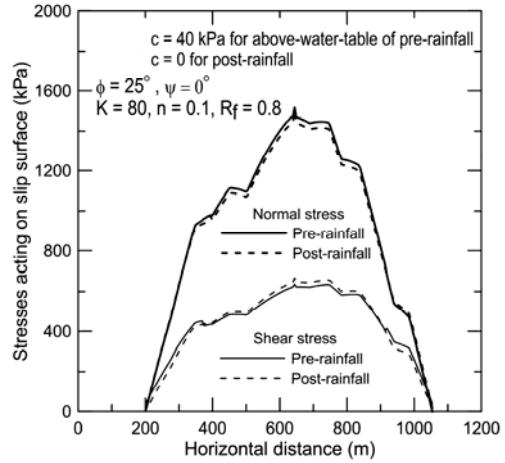

(a) Normal and shear stresses

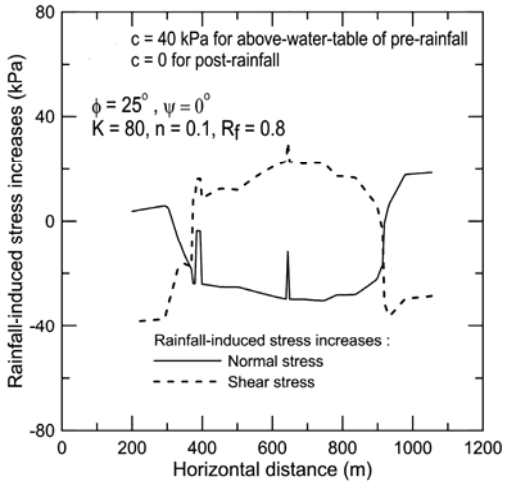

(b) Stress increments

Fig. 12 Stress distribution on the failure surface for ψ = 0°

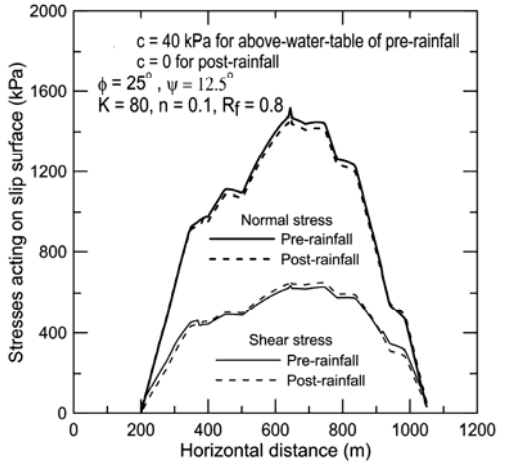

(a) Normal and shear stresses

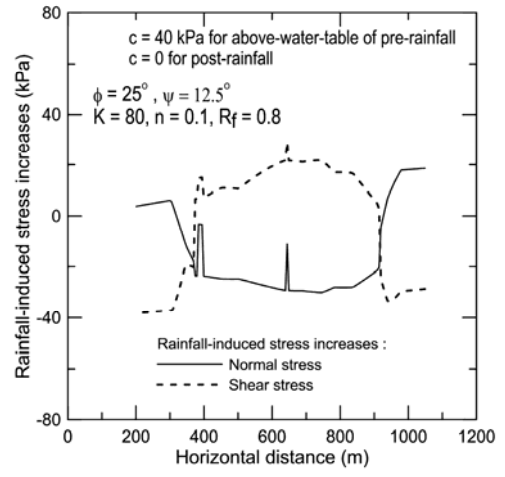

(b) Stress increments

Fig. 13 Stress distribution on the failure surface for ψ = 12.5°

6. DISCUSSIONS

Engineering judgments regarding "stability" and "instability" of slopes based on conventional limit equilibrium methods are impractical, in the sense that a stable slope from conventional point of view may be associated a certain displacement; an unstable slope from conventional point of view may be associated with a limited (or remediable) slope displacement. Rather than providing conventional thresholds of slope stability (namely, F_s = 1.0), the proposed method provides new thresholds of slope stability from both stress and displacement viewpoints. The present study constitutes the first step of using new local stress- and displacement-based slope stability criteria. Also noted that the present method is an extension of limit-equilibrium-based slice method, which inherits some characters of conventional slice methods, e.g., the use of a potential failure surface as a priori. One may question the legitimacy of using a pre- existing failure surface, instead of a progressively generated failure surface as commonly seen in the analytical outcome of Finite element method (FEM). It is noted, however, a progressively generated failure surface (as seen in FEM) can be deemed as a part of a potential failure surface for which the displacement compatibility within the sliding mass is satisfied (as in the proposed method). This method is not intended to replace widely available FEM methods, and is intended to provide alternative tools to solve slope engineering problems with varieties of geological uncertainty and unknowns. Because the present method employs a stress vs. displacement constitutive soil model which differs from the stress vs. strain model used in the FEM, a direct comparison between these two methods is difficult and is beyond the scope of this study. Also note that the soil parameters (c = 0 for post-rainfall; c = 40kPa for pre-rainfall, and ϕ = 25°, ψ = 0°, K = 80, n = 0.1, R_f = 0.8 for pre- and post-rainfall cases) used for deriving Figs. 9 ~ 12 were back-calculated from the studied slope based on a known potential sliding surface. These parameters are slightly different from those reported by Huang (2013) for the same slope (c = 0 for post-rainfall; c = 40kPa for pre-rainfall, ϕ = 26°, ψ = 0°, K = 90, n = 0.2, R_f = 0.8) based on rigorous Janbu's method (Janbu 1973) and a non-circular failure surface. Due to the differences in the context of force-equilibrium and shape of sliding surface, results of back-analyses were slightly different, yet both sets of soil parameters generate similar values of slope displacement of about 0.03 m at the location of X = 784m.

7. CONCLUSIONS

A novel improvement on conventional limit-equilibrium-based slope stability analysis was achieved here, providing significant information regarding the displacement of the slope subjected to internal and/or external environmental changes. The proposed force-equilibrium-based finite displacement methods (FFDM) were formulated based on force and moment equilibrium adopted in the simplified Bishop's and Fellenius' methods, incorporating as displacement compatibility requirement and a hyperbolic shear stress-displacement soil model. A static determinate condition was attained by introducing displacement compatibility functions and hyperbolic shear stress-displacement relationships for the slope materials. As a result, local displacement-based and stress-based safety factors along the potential failure surface are parts of the analytical solution. Based on the case study of a well-monitored slope during a rainstorm, the effect of a rise in the groundwater table during the rainstorm, expressed as an incremental slope displacement, was computed using the proposed FFDM. It was shown that the slope displacement measured during the rainstorm can be closely simulated using stress vs. displacement relationships relevant to the data obtained from large-scale direct shear tests (Huang 2013a, b), revealing the potential of the present method for further applications. Results of a comparative study also reveals that using Fellenius' method of limit equilibrium tends to render conservative values of slope displacements, due partially to its less realistic assumptions on the inter-slice forces. The slope displacement calculated using simplified Bishop's approach of limit equilibrium is comparable with that measured for the studied slope subjected to a groundwater table rise. Consequently, the Bishop's method of limit equilibrium is suggested for further applications of FFDM in the future.

REFERENCES

Atkinson, J.H. (1981). *Foundations and Slopes: An Introduction to Applications of Critical State Soil Mechanics*. McGraw-Hill, London.

Bjerrum, L. (1967). "Progressive failure in slopes of overconsolidated plastic clay and clay shales." *Journal of the Soil Mechanics and Foundations Division*, ASCE, **93**, 1–49.

Bishop, A.W. (1955). "The use of the slip circle in the stability analysis of slopes." *Geotechnique*, **5**, 7–17.

Chang, M., Chiu, Y., Lin, S., and Ke, T.-C. (2005). "Preliminary study on the 2003 slope failure in Woo-Wan-Chai area, Mt. Ali Road, Taiwan." *Engineering Geology*, **80**, 93–114.

Ching, R.K.H. and Fredlund, D.G. (1983). "Some difficulties associated with the limit equilibrium method of slices." *Canadian Geotechnical Journal*, **20**, 661–672.

Clough, G.W. and Duncan, J.M. (1971). "Finite element analyses of retaining wall behavior." *Journal of Soil Mechanics and Foundation Division*, ASCE, **97**(SM12), 1657–1673.

Cole, E.R.L. (1967). "The behavior of soils in the simple shear apparatus." *Ph. D. Dissertation*, University of Cambridge.

Duncan, J.M. and Chang, C.-Y. (1970). "Nonlinear analysis of stress and strain in soils." *Journal of Soil Mechanics and Foundation Division*, ASCE, **96**(SM5), 1629–1653.

Duncan, J.M., Byrne, P., Wong, K.S., and Mabry, P. (1980). "Strength, stress-strain and buck modulus parameters for finite element analyses of stresses and movements in soil masses." Report No. VCB/GT/80-01, Department of Civil Engineering, University of California at Berkeley, August, 77.

Duncan, J.M. and Wright, S.G. (2005). *Soil Strength and Slope Stability*. *Chapter 6: Mechanics of Limit Equilibrium Procedures*. John Wiley & Sons Ltd., 55–102.

Energy and Resources Research Laboratory (ERRL) of Industrial Technology Research Institute (1999). "Report on the site exploration for Wu-Wan-Zai landslide area in Chia-Yi County." The Fifth Maintenance Office, Directorate General of Highways, Ministry of Transportation and Communications.

Fan, C.C. and Chen, Y.W. (2010). "The effect of root architecture on the shearing resistance of root-permeated soils." *Ecological Engineering*, **36**, 813–826.

Fellenius, W. (1936). "Calculation of the stability of earth dams." *Proceedings of 2nd Congress on Large Dams*, **4**, pp. 445–463.

Fredlund, D.G. and Krahn, J. (1977). "Comparison of slope stability methods of analysis." *Canadian Geotechnical Journal*, **25**, pp. 238–249.

Huang, C.C. (2013a). "Developing a new slice method for slope displacement analyses." *Engineering Geology*, **157**, 39–47.

Huang, C.C. (2013b). "Formulation and verification of force- equilibrium-based finite displacement method (FFDM) for slope stability analysis." *Keynote Lecture in the 15th Conference on Current Researches in Geotechnical Engineering in Taiwan. Yunlin*, Taiwan, September 11–13.

Janbu, N. (1973). *Slope Stability Computations, Embankment-Dam Engineering*. Casagrande Volume, John Wiley & Sons, 47–86.

Jewell, R.A. and Wroth, C.P. (1987). "Direct shear tests on reinforced sand." *Geotechnique*, **37**(1), 53–68.

Leshchinsky, D. (1990). "Slope stability analysis: Generalized approach." *Journal of Geotechnical Engineering*, **116**(5), 851–867.

Leshchnisky, D. and Huang, C.-C. (1992). "Generalized slope stability analysis: Interpretation, modification, and comparison." *Journal of Geotechnical Engineering*, **118**(10), 1559–1576.

Morgenstern, N.R. and Price, V.E. (1965). "The analysis of the stability of general slip surfaces." *Geotechnique*, **15**, 9–93.

Oda, M. (1975). "On stress-dilatancy relation of sand in simple shear test." *Soils and Foundations*, **18**(2), 17–29.

Sarma, S.K. (1973). "Stability analysis of embankments and slopes." *Geotechnique*, **23**(3), 423–433.

Spencer, E. (1973). "Thrust line criterion in embankment stability analysis." *Geotechnique*, **23**(1), 85–100.

Whitman, R.V. and Bailey, W.A. (1967). "Use of computers for slope stability analysis." *Journal of the Soil Mechanics and Foundation Division*, ASCE, **93**(SM4), 475–497.